Three-Dimensional Structure of Tidal Current in the East China Sea and the Yellow Sea

Xinyu Guo[1] and Tetsuo Yanagi[2]

[1]*Institute for Global Change Research,*
  SEAVANS North 7F, 1-2-1 Shibaura, Minato, Tokyo 105-6791, Japan
[2]*Research Institute for Applied Mechanics, Kyushu University,*
  6-1 Kasuga-kohen, Kasuga, Fukuoka 816-8580, Japan

A three-dimensional tidal current model is developed and applied to the East China Sea (ECS), the Yellow Sea and the Bohai Sea. The model well reproduces the major four tides, namely M_2, S_2, K_1 and O_1 tides, and their currents. The horizontal distributions of the major four tidal currents are the same as those calculated by the horizontal two-dimensional models. With its high resolutions in the horizontal (12.5 km) and the vertical (20 layers), the model is used to investigate the vertical distributions of tidal current. Four vertical eddy viscosity models are used in the numerical experiments. As the tidal current becomes strong, its vertical shear becomes large and its vertical profile becomes sensitive to the vertical eddy viscosity. As a conclusion, the HU (a) model (Davies *et al.*, 1997), which relates the vertical eddy viscosity to the water depth and depth mean velocity, gives the closest results to the observed data. The reproduction of the amphidromic point of M_2 tide in Liaodong Bay is discussed and it is concluded that it depends on the bottom friction stress. The model reproduces a unique vertical profile of tidal current in the Yellow Sea, which is also found in the observed data. The reason for the reproduction of such a unique profile in the model is investigated.

1. Introduction

As one of the most important physical processes in the East China Sea (ECS) and the Yellow Sea, the tide and tidal current there have been investigated by field observation data (Ogura, 1933; Nishida, 1980; Larsen *et al.*, 1985; Fang, 1986), satellite altimetric data (Yanagi *et al.*, 1997) and numerical models (An, 1977; Shen, 1980; Choi, 1980, 1984, 1989; Ding, 1984; Yanagi and Inoue, 1994; Zhao *et al.*, 1994; Ye and Mei, 1995). It may be stated that the general information about the tidal dynamics in this region is now available. However, since we have few observed tidal current data, and most numerical models are horizontally two-dimensional ones, the three-dimensional structure of tidal current in this region is little known and must be investigated more thoroughly.

Among the numerical models of the tide and tidal current in the ECS, some are based on the boundary value method (Shen, 1980; Ding, 1984), which calculates the tide in the domain based on the harmonic constants along the coast and ignores the nonlinear effects. Usually there are not enough tide gauges to provide the harmonic constants along the coast of the model domain, and so the use and precision of the boundary value method are limited.

The other models are based on the initial value method (An, 1977; Choi, 1980, 1984, 1989; Yanagi and Inoue, 1994; Zhao *et al.*, 1994; Ye and Mei, 1995), which reproduces the tide in the domain from the harmonic constants along the open boundary, according to the physical rule. Some available harmonic constants along the coast of the domain are used to verify the model's results. Therefore, this method is more logical and has recently become popular.

Table 1, which summarizes the main characteristics of the tidal models in the ECS, the Yellow Sea and the Bohai Sea based on the initial value method, shows that most tide models are horizontally two-dimensional ones with a horizontal resolution of about 25 km. All of the two-dimensional models include the nonlinear advective terms, while the three-dimensional models (Choi, 1984, 1989) ignore them. The horizontal eddy viscosity is said to have little influence on the tide because it acts as a scale-selective filter, damping the shorter waves more heavily than the long waves (Davies *et al.*, 1997). Including it or not in the tide model should thus not be a serious problem. The effect of the tide generating potential on the M_2 tide in this region is said to be less than 3% (An, 1977) and is usually ignored. The effect of the earth's curvature on the tide in this region is also said to be small enough to be ignored in the numerical model (Yanagi and Inoue, 1994).

Table 1. Summary of the tidal models in the East China Sea, the Yellow Sea and the Bohai Sea, in which Y = Yellow Sea; B = Bohai Sea; E = East China Sea; Four = M_2, S_2, K_1 and O_1 tides; ADV = advective terms; HEV = horizontal eddy viscosity (cm^2s^{-1}); GF = tide-generating force; C_b = sea bed drag coefficient; Lat = latitude; Long = longitude; 2-D = horizontally two-dimensional model; 3-D = three-dimensional model.

Authors	Domain	Tide	DIM	Mesh size	ADV	HEV	GF	C_b
An(1977)	Y,B	M_2	2-D	11 km	Yes	10^6	Yes	0.0026
Choi(1980)	E,Y,B	Four	2-D	1/5°Lat 1/4°Long	Yes	No	No	0.0025
Choi(1984)	E,Y,B	M_2	3-D	1/5°Lat 1/4°Long	No	No	No	0.0025
Choi(1989)	E,Y,B	M_2	3-D	1/15°Lat 1/12°Long	No	No	No	0.0030
Yanagi and Inoue(1994)	E,Y,B	Four	2-D	25 km	Yes	10^7	No	0.0026
Zhao et al.(1994)	E,Y,B	Four	2-D	1/4°	Yes	10^8	Yes	0.001-0.0035
Ye and Mei(1995)	E,Y,B	Four	2-D	1/4°	Yes	No	Yes	0.0017-0.0055
Guo and Yanagi	E,Y,B	Four	3-D	12.5 km	Yes	10^7	No	0.0015-0.0030

The calculation of the bottom friction stress may be the most important problem in the tide model. The quadratic friction rule is often used; that is, the bottom friction stress is calculated from the velocity at a single height (for example, 1 m above the sea bottom) and a constant, i.e. the bed drag coefficient. In the two-dimensional model, the velocity at a single height has to be replaced by the depth mean velocity, while in the three-dimensional model this velocity is represented by the velocity of the layer nearest to the sea bottom or the depth mean velocity (Davies *et al.*, 1997). A widely used value for the bed drag coefficient is 0.0026. In the numerical models for the tide and tidal current in the ECS, the Yellow Sea and the Bohai Sea, 0.0026 or a value close to it were used by An (1977), Choi (1980, 1984, 1989) and Yanagi and Inoue (1994). However, Chinese scientists prefer a small value for this coefficient. Zhao *et al.* (1994) assumed that the bed drag coefficient has a horizontal variation, using values of 0.001 west to the line from (40°N, 124.25°E) to (25°N, 120.75°E), 0.0035 in the Korea/Tsushima Strait and 0.0016 in the remaining region; while Ye and Mei (1995) used different bed drag coefficients to simulate different tides (0.0017 for M_2 tide, 0.0051 for S_2 tide, 0.0055 for K_1 and O_1 tides). Using such small values for M_2 tide, the model can well reproduce the amphidromic point in Liaodong Bay, while the models using 0.0026 cannot reproduce this amphidromic point.

Few three-dimensional tide models have been reported for the ECS, the Yellow Sea and the Bohai Sea. Choi (1984) developed a linear three-dimensional model with three layers in the vertical. However, compared to his horizontal two-dimensional model with the same horizontal resolution and topography data (Choi, 1980), the tide reproduced by the three-dimensional model is not very good, especially in the Bohai Sea. To solve this problem, Choi (1989) improved the model's horizontal resolution and ran the same model again. Though the results are better than before, the tidal amplitude in the Bohai Sea is still underestimated and the amphidromic point in Liaodong Bay is not reproduced. And, since his

model has only three layers in the vertical, the vertical variation of tidal current cannot be resolved very clearly.

Summarizing the above tide models of the ECS, the Yellow Sea and the Bohai Sea, it can be said that there is still no complete three-dimensional tide model that can clarify the three-dimensional structure of the tidal current in this region. Here, we present a high resolution (12.5 km × 12.5 km × 20 layers) three-dimensional tide model to investigate this problem. The open boundary is located out of the Ryukyu Islands in order to include the shelf edge in the model. Four major tides, namely M_2, S_2, K_1 and O_1 tides, are chosen to be reproduced. After reproducing the four tides and tidal currents, more attention is paid to the vertical distribution of tidal current and the influence of the bottom friction stress and interior friction on the tidal current.

2. Numerical Model

Because the effect of the earth's curvature on the tidal phenomena in the ECS and the Yellow Sea is small enough to be ignored in a numerical model (Yanagi and Inoue, 1994), we formulate our problem in the Cartesian coordinate system. Assuming constant density, the tide and tidal current are controlled by the following equations, in which the x axis is eastward, y axis northward, and z axis upward from the mean sea surface.

$$\frac{\partial u}{\partial t} + \vec{u} \cdot \nabla u - fv = -g\frac{\partial \eta}{\partial x} + \frac{\partial}{\partial z}\left(A_v \frac{\partial u}{\partial z}\right) + A_h\left(\frac{\partial^2 u}{\partial x^2} + \frac{\partial^2 u}{\partial y^2}\right), \quad (1)$$

$$\frac{\partial v}{\partial t} + \vec{u} \cdot \nabla v - fu = -g\frac{\partial \eta}{\partial y} + \frac{\partial}{\partial z}\left(A_v \frac{\partial v}{\partial z}\right) + A_h\left(\frac{\partial^2 v}{\partial x^2} + \frac{\partial^2 v}{\partial y^2}\right), \quad (2)$$

$$\frac{\partial \eta}{\partial t} + \frac{\partial}{\partial x}\int_{-h}^{0}udz + \frac{\partial}{\partial y}\int_{-h}^{0}vdz = 0. \quad (3)$$

Here u and v are the eastward and northward velocity,

respectively; η the sea surface elevation from the mean sea surface; $f = f_0 + \beta y$ ($f_0 = 7.73 \times 10^{-5}$ s^{-1} at 32°N, $\beta = 1.94 \times 10^{-13}$ s^{-1}cm^{-1}) the Coriolis parameter; g (=980 cm s^{-2}) the gravitational acceleration; A_h (=10^7 cm^{2}s^{-1}, Yanagi and Inoue, 1994) the horizontal eddy viscosity; h the water depth.

The vertical eddy viscosity A_v represents the interior friction of tidal current and may have a large effect on the calculated tidal current near the sea bottom (Davies *et al.*, 1997). Many models of the vertical eddy viscosity have been used in the tidal calculations, from a simple constant model to the turbulence energy model (Xing and Davies, 1996). In this paper, we use four models described below to determine the vertical eddy viscosity. By comparing the results of these models, we want to find the best one suitable for the tidal calculation in the ECS, the Yellow Sea and the Bohai Sea.

The first model is to set the vertical eddy viscosity as a constant (50 cm^2/s).

The second model is the mixing length model (Fang and Ichiye, 1983) and expressed as:

$$A_v = l^2 \sqrt{\left(\frac{\partial u}{\partial z}\right)^2 + \left(\frac{\partial v}{\partial z}\right)^2}. \qquad (4)$$

The mixing length l is defined as:

$$l(z) = \kappa(z+h)\left(1 - \frac{z+h}{(1+s)h}\right), \qquad (5)$$

where κ (=0.4) is the Von Kármán's constant, s (=1.2) a parameter expressing the roughness of the sea surface (Fang and Ichiye, 1983).

The third and fourth models relate A_v to the water depth and the vertical mean velocity (Davies *et al.*, 1997), as:

$$A_v = 2.5 \times 10^{-3} h \sqrt{\left(\overline{u}^2 + \overline{v}^2\right)} \Phi(z) \qquad (6)$$

where $\Phi(z)$ is a function of the depth. In the third model, it is set to a constant (=1) and this model is referred to model HU (a). In the fourth model, it is set to:

$$\Phi(z) = \begin{cases} 1 & \text{if } -h_0 \leq z \\ \dfrac{z+h-(z+h_0)\mu_0}{h-h_0} & \text{if } -h \leq z < -h_0. \end{cases} \qquad (7)$$

Referring to Davies *et al.* (1997), h_0 is set to 0.9 h, μ_0 is set to 0.2. This model will be called model HU (b) in this paper.

The stress at the sea surface is assumed to be zero and the stress at the sea bottom is calculated by:

$$A_v \frac{\partial(u,v)}{\partial z} = \frac{1}{\rho}\left(\tau_b^x, \tau_b^y\right) = C_{100}\left(u_{100}, v_{100}\right)\sqrt{u_{100}^2 + v_{100}^2} \qquad (8)$$

where u_{100} and v_{100} are the velocity 1 m above the sea bottom in the eastward and northward direction, respectively. C_{100} is the bed drag coefficient.

As pointed out by Davies *et al.* (1997), the bottom friction stress in the three-dimensional model may also be calculated from the depth mean velocity, similarly to that in the horizontally two-dimensional model, as:

$$A_v \frac{\partial(u,v)}{\partial z} = \frac{1}{\rho}\left(\tau_b^x, \tau_b^y\right) = C_b\left(\overline{u}, \overline{v}\right)\sqrt{\overline{u}^2 + \overline{v}^2} \qquad (9)$$

where $\overline{u}$ and $\overline{v}$ are the depth mean velocity in the eastward and northward direction, respectively. C_b is a coefficient similar to C_{100}.

Due to the vertical resolution of the three-dimensional model, the velocity 1 m above the sea bottom is difficult to calculate in the model, and the velocity of the layer nearest to the sea bottom (hereafter referred to the bottom layer) is often used to replace it. However, no matter what coordinate system is used (z or σ coordinate) in the numerical model, this approximation means that the height of u_{100} and v_{100} above the sea bottom varies with the water depth. At some shallow places, the height of u_{100} and v_{100} may be less than 1 m, while at some deep places it may be larger than 1 m. In fact, the error of the topography data is usually even larger than 1 m. Therefore, the calculation of u_{100} and v_{100} in a three-dimensional model is very difficult.

The topography of the model's domain is shown in Fig. 1, in which the depth data are read from the chart. Depths greater than 1000 m are set to 1000 m. This approximation should have little influence on the propagation of tidal wave. The grid size is 12.5 km × 12.5 km and the water column is divided into 20 vertical layers.

The positions of the tide gauges and the corresponding grids are plotted in the same figure. The harmonic constants for the major four tides can be found in Choi (1980) and will be used to check our model's results. Due to the limited horizontal resolution, the positions of the corresponding grids of tide gauges are somewhat different from their actual positions. Apart from these tide gauges, some tidal current observation stations are also shown in Fig. 1. Tidal current data for these can be found in Larsen (1985) and Choi (1984, 1985, 1989). Table 2 summarizes these data, including the station position, observation period, depth and the analyzed harmonic constant of tidal current. It should be noted that due to the horizontal and vertical resolution limitation, there is a possibility that the depth of the corresponding grid is a little different from the recorded station depth.

The above equations are solved by the finite difference method (Guo and Yanagi, 1994). The open boundary is

Table 2. Observed tidal current data in Larsen *et al.* (1985), Choi (1984, 1985, 1989), in which the amplitude of tidal current (H) is in cm/s and the local phase lag κ in degree and referred to longitude of current meter mooring stations.

Station	Lat.	Long.	Date (day/year)	Depth (m)	M2 U H	M2 U κ	M2 V H	M2 V κ	S2 U H	S2 U κ	S2 V H	S2 V κ	K1 U H	K1 U κ	K1 V H	K1 V κ	O1 U H	O1 U κ	O1 V H	O1 V κ
M2	31.39	122.37	(214-226)/81	4	84.0	104	83.4	99	32.5	151	32.7	35	9.7	335	10.3	285	10.9	278	10.1	247
				13	36.5	64	46.1	309	16.9	127	16.6	356	5.2	201	6.4	320	2.8	133	3.9	273
M5	32.00	124.50	(215-224)/81	5	55.0	133	58.7	44	22.0	197	24.4	102	29.7	333	30.6	248	24.7	298	23.7	208
				20	47.3	57	50.8	321	17.4	120	17.8	16	4.5	58	8.2	313	5.4	6	7.9	266
				35	39.1	93	40.1	355	16.8	145	16.3	40	2.4	89	5.0	339	2.8	33	4.8	285
M7	30.33	123.44	(216-225)/81	5	39.7	63	43.1	312	13.7	87	16.5	350	21.4	324	17.0	249	14.7	272	8.5	203
				50	24.0	40	34.6	286	7.9	94	12.0	324	1.2	291	4.2	16	0.4	103	3.7	318
				60	19.1	71	26.9	311	7.1	119	10.1	354	1.6	285	3.0	26	0.9	143	3.4	328
MS	30.52	124.80	(155-175)/80	23	42.2	34	40.7	296	11.9	65	10.2	322	5.8	329	7.7	260	4.4	330	6.0	240
				32	35.5	11	33.8	271	10.3	39	9.4	301	3.2	306	4.0	259	2.7	329	4.0	250
				45	31.8	22	30.0	282	9.3	46	8.7	309	2.7	312	3.9	305	2.6	335	4.1	258
CM7	28.65	125.45		20	31.0	2	23.0	240	16.0	53	10.0	288	3.0	260	2.0	130	1.0	130	2.0	2
SB	28.91	127.25	(155-186)/80	177	26.7	6	16.8	226	4.7	22	4.3	232	1.1	230	2.1	147	0.8	262	1.0	227
B	36.95	124.08	(13-72)/86	38	18.6	4	32.8	146	7.9	72	12.2	200	2.4	144	5.9	272	1.4	102	3.9	237
				74	11.8	12	22.4	136	5.3	73	8.6	191	1.8	147	3.7	272	1.3	110	2.1	242
D	36.00	124.58	(12-71)/86	41	15.2	11	26.1	63	7.6	79	12.2	113	1.5	220	8.8	257	0.9	169	5.9	213
				86	15.5	10	17.0	60	7.5	72	7.2	109	2.0	169	5.1	262	1.2	121	3.6	225
F	35.23	124.74	(13-72)/86	70	5.0	7	40.0	19	2.7	90	19.6	71	2.4	127	10.4	252	2.4	54	7.3	211
				94	8.4	329	26.0	350	4.3	57	12.1	66	2.1	147	6.6	251	1.6	51	4.8	190
I	34.30	124.69	(12-41)/86	48	13.4	112	43.8	359	7.1	164	18.4	54	2.7	79	12.7	253	2.7	42	8.4	207
C	36.95	125.41	(12-65)/86	52	29.5	4	26.0	88	12.8	69	11.0	142	2.7	153	4.8	259	1.8	108	3.1	220
E	36.03	125.60	(13-72)/86	63	20.2	348	25.4	43	8.9	49	11.9	95	1.7	164	5.5	242	1.4	118	3.4	203
M4	31.25	122.82	(322-332)/81	2	47.0	95	48.0	325	17.0	100	20.5	330	2.6	302	11.1	289	4.0	200	8.9	254
				25	40.1	86	40.6	316	16.4	127	16.5	351	5.4	230	9.4	330	4.1	154	6.1	280
				38	34.8	77	35.6	305	12.6	121	12.8	340	6.9	227	7.5	313	4.7	157	4.6	250
				44	30.0	74	33.7	301	10.7	119	11.9	336	6.5	227	6.4	318	4.5	157	4.1	253
SDS80	31.46	123.50	(156-179)/80	999	20.1	5	29.5	273	5.9	36	10.4	306	2.4	241	4.0	277	2.7	205	2.7	250
SDS81	31.16	122.46	(216-226)/81	999	12.4	53	23.3	296	3.0	76	9.2	331	3.1	200	3.3	337	1.1	77	3.0	284
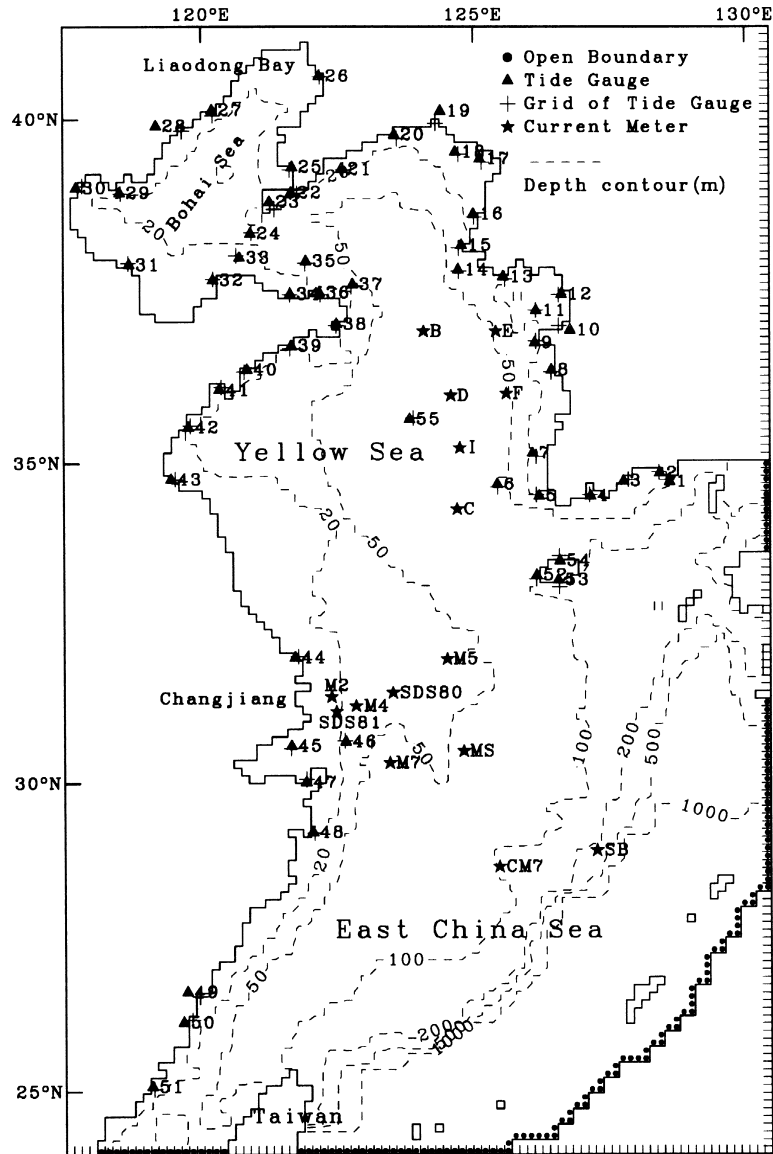
Fig. 1. The topography of the East China Sea, the Yellow Sea and the Bohai Sea. The positions of the open boundary, tidal gauges and their corresponding grids, and the observed tidal current data are shown by the black circles, black triangles, plus symbol and black stars, respectively.

located at the Taiwan Strait, offshore of Ryukyu Islands and the Korea/Tsushima Strait (Fig. 1), along which the known tidal harmonic constants are given. The necessary harmonic constants along the open boundary are read from the co-tidal and co-range charts presented by Nishida (1980). The major four tides of M_2, S_2, K_1 and O_1 are selected for reproduction. The calculations for these tides last for five periods and the harmonic analysis is done in the last period.

3. Result

To clarify the response of the model to the parameters, we designed 12 case runs for each tide, as shown in Table 3.

At first, the bed drag coefficient is changed from 0.0030 to 0.0010 to find the most suitable value (case 1–case 5). Then different vertical eddy viscosity models are used (case 6–case 12). The bottom friction stress is calculated from the depth mean velocity (case 1–case 8) and the velocity of the bottom layer (case 9–case 12), respectively.

The calculated results are compared with the observed data in three ways. The first way is to compare the calculated harmonic constants of tidal elevation with the observed ones at 55 tide gauge stations (Choi, 1980). A parameter H_s, defined in Davies *et al.* (1997), is used in the comparison,

Table 3. Calculated cases for M_2, S_2, K_1 and O_1 tides.

Case	τ_b	Sea bed drag coefficient				A_v
		M_2	S_2	K_1	O_1	
1	Eq. (9)	0.0030	0.0030	0.0030	0.0030	50 cm^2/s
2	Eq. (9)	0.0025	0.0025	0.0025	0.0025	50 cm^2/s
3	Eq. (9)	0.0020	0.0020	0.0020	0.0020	50 cm^2/s
4	Eq. (9)	0.0015	0.0015	0.0015	0.0015	50 cm^2/s
5	Eq. (9)	0.0010	0.0010	0.0010	0.0010	50 cm^2/s
6	Eq. (9)	0.0015	0.0030	0.0030	0.0030	Mixing length
7	Eq. (9)	0.0015	0.0030	0.0030	0.0030	HU (a)
8	Eq. (9)	0.0015	0.0030	0.0030	0.0030	HU (b)
9	Eq. (8)	0.0015	0.0030	0.0030	0.0030	50 cm^2/s
10	Eq. (8)	0.0015	0.0030	0.0030	0.0030	Mixing length
11	Eq. (8)	0.0015	0.0030	0.0030	0.0030	HU (a)
12	Eq. (8)	0.0015	0.0030	0.0030	0.0030	HU (b)

Table 4. Comparison between the observed and calculated M_2, S_2, K_1 and O_1 tides and tidal currents, in which H_s defined by Eq. (10); H = water elevation; U = u-component of tidal current; V = v-component of tidal current; A = Amphidromic points of M_2 and S_2 tides in Liaodong Bay.

Case	M_2				S_2				K_1			O_1		
	H_s-H	H_s-U	H_s-V	A	H_s-H	H_s-U	H_s-V	A	H_s-H	H_s-U	H_s-V	H_s-H	H_s-U	H_s-V
1	65.2	24.9	30.4	No	23.2	9.2	10.5	Yes	13.6	5.6	5.6	7.8	4.6	4.1
2	63.4	22.9	28.9	No	24.0	9.6	10.4	Yes	14.2	5.8	5.7	8.2	4.7	4.3
3	62.0	19.2	27.2	No	25.3	10.2	12.1	Yes	14.9	6.0	5.8	8.7	4.8	4.5
4	61.4	19.2	23.1	Yes	27.2	11.0	10.8	Yes	16.0	6.3	5.9	9.4	5.0	4.8
5	63.0	19.2	21.7	Yes	30.3	12.1	11.5	Yes	17.8	6.8	6.2	10.4	5.1	5.1
6	89.6	20.3	20.0	No	30.6	10.1	9.5	Yes	16.4	5.2	6.5	7.8	4.6	4.0
7	61.8	19.2	20.8	Yes	23.1	9.1	9.6	Yes	12.7	5.7	6.0	7.7	4.6	3.9
8	65.5	13.3	18.8	No	23.8	7.4	8.9	Yes	13.2	4.7	5.6	7.0	4.1	3.6
9	70.9	22.0	24.0	Yes	28.7	11.3	10.8	Yes	14.2	6.4	6.4	9.3	5.0	4.6
10	68.6	13.7	19.3	No	24.8	8.1	9.8	Yes	13.5	5.7	6.2	7.6	4.8	4.3
11	62.6	21.4	23.0	Yes	25.6	10.7	10.7	Yes	13.9	6.3	6.3	9.0	5.0	4.4
12	61.5	17.3	21.4	Yes	24.4	9.3	10.2	Yes	13.7	5.8	6.1	8.3	4.7	4.3

$$H_s = \frac{1}{N} \sum_{i=1}^{N} \sqrt{\left(HC_i^2 + HS_i^2 \right)} \quad (10)$$

$$HC = A_o\cos(\alpha_o) - A_c\cos(\alpha_c)$$

$$HS = A_o\sin(\alpha_o) - A_c\sin(\alpha_c)$$

where, A_o and α_o are the observed tidal amplitude and phase at the tide gauge station; A_c and α_c the calculated ones at the stations for comparison. Values of H_s for the 12 cases are shown in Table 4.

The second way is the comparison of the calculated tidal current with the observed data summarized in Table 2.

Similarly, the H_s of the u and v components of the tidal current are calculated and also shown in Table 4.

The third way is the comparison of the co-tidal and co-range charts based on the observed data and calculated results (Fig. 2). Since some cases cannot reproduce the amphidromic point of M_2 tide in Liaodong Bay, the appearance or not of this amphidromic point is presented in Table 4 too.

3.1 Comparison of the model results and observed data
3.1.1 M_2 tide

Since many papers have suggested the existance of the amphidromic point in Liaodong bay (Ogura, 1933; Nishida, 1980; Fang, 1986) and some models have failed to reproduce

it (Choi, 1980, 1984, 1989; Yanagi and Inoue, 1994), whether or not it is reproduced will be an important factor in choosing the model parameters. With the decrease of the bed drag coefficient (0.0030 to 0.0015), the calculated M_2 tidal elevation along the coast increases and H_s-H, the difference between the simulated and observed data, becomes small, as shown in Table 4. As the bed drag coefficient is equal to 0.0015, the amphidromic point in Liaodong Bay begins to appear. If the bed drag coefficient decreases further, H_s-H becomes large again, but the amphidromic point in Liaodong bay can be reproduced clearly. Therefore, the bed drag coefficient for M_2 tide simulation is decided as 0.0015.

Using the same bed drag coefficient (0.0015), the constant (case 4) and HU (a) vertical eddy viscosity models can reproduce the amphidromic point in Liaodong Bay while the mixing length and HU (b) models cannot. Furthermore the H_s-H of the former two cases are smaller than the latter two cases. However, as for the reproduction of the tidal current, the mixing length and HU (b) models are better than or at least as good as the constant and HU (a) models. Therefore the decrease of the vertical eddy viscosity near the sea bottom in the mixing length and HU (b) models seems to be good for the reproduction of tidal current, especially that near the sea bottom, but not good for the tidal elevation.

Instead of Eq. (9), Eq. (8) is used to calculate the bottom friction stress in cases 9–12. Obviously, the influence of the bottom friction stress on the reproduced vertical profile of the tidal current becomes more important since the velocity of the bottom layer is used to calculate the bottom friction stress directly. From Table 4, we see that cases 9 and 11 give worse results than cases 4 and 7, while cases 10 and 12 give better results than cases 6 and 8. The reason for this difference is thought to be that the models with the decreasing eddy viscosity near the sea bottom better reproduce the tidal current near the sea bottom than the vertically constant eddy viscosity models.

3.1.2 S_2 tide

The simulation of the S_2 tide shows a different response to the change of the bed drag coefficient than M_2 tide simulation. The decrease of the bed drag coefficient from 0.0030 causes the model results to deviate further from the observed results. The amphidromic point in Liaodong Bay can be reproduced in all cases. As the bed drag coefficient increases above 0.0030 (not shown here), the amphidromic point becomes unclear and H_s for the tidal currents also increases. Therefore the bed drag coefficient for S_2 tide simulation was decided to be 0.0030.

As the vertical eddy viscosity model and the bottom friction stress calculation are changed, the S_2 tide simulation is not so sensitive as the M_2 tide simulation. However, the mixing length model gives worse result than the other models.

3.1.3 K_1 and O_1 tides

K_1 and O_1 tide simulations show the same response to the change of the bed drag coefficient and their responses are similar to S_2 tide simulation. A value of 0.0030 is used in these two tide simulations.

With the exception of the mixing length model, the other three vertical eddy viscosity models do not give very different results. This is because these components of tidal currents are weak and their vertical shears are small, compared to the M_2 tidal currents. The reason for the poor result of the mixing length model will be mentioned below.

3.2 Co-tidal and co-range charts

Figure 2 shows the observed co-tidal and co-range charts of M_2, S_2, K_1 and O_1 tide (Nishida, 1980) and the calculated values according to case 7. As for the M_2 and S_2 tides (Figs. 2(a) and (b)), except for the Bohai Sea, where the amplitude is underestimated, the calculated results are well consistent with the observed ones. Four amphidromic points are reproduced, in which the positions of two amphidromic points in the Yellow Sea are almost the same as the observed ones, while some deviation exists in the positions of the other two amphidromic points in the Bohai Sea, which may be attributed to the model's resolution, which cannot represent the coast and topography well.

As for the K_1 and O_1 tides (Figs. 2(c) and (d)), also except for the Bohai Sea, where the amplitude is overestimated, the model reproduces the observed data well. Referring the model results of M_2 and S_2 tides, it can be concluded that our model tends to underestimate the semi-diurnal tides in the Bohai Sea but to overestimate the diurnal tides there. The same trend also exists in the results of the horizontally two-dimension model (Yanagi and Inoue, 1994), whose topography data is the same as that used in the present model. Therefore the error in reading depth data from the chart and the choice of the grids along the coast line may be a possible reason for such under- or over-estimation.

3.3 The horizontal distribution of tidal current

Figure 3 shows the horizontal distribution of tidal current ellipses of four major tides at the sea surface. Basically, the distributions of M_2 and K_1 tidal currents are similar to those of S_2 and O_1, respectively. The strongest semi-diurnal tidal currents appear at the offshore area of Changjiang River Mouth and the western Korean coast, while the strongest diurnal tidal currents appear in Bohai Sea. Note that the major and minor axes of the M_2 and S_2 tidal current ellipses at the offshore area of Changjiang River Mouth are nearly the same, so the tidal mixing there is therefore strong at any time. But on the continental shelf (water depth less than 200 m), the major axis is clearly longer than the minor axis, which means that the tidal mixing across the depth contour is stronger than that along it.

The horizontal distributions of tidal currents presented here are nearly the same as those calculated by the horizontal
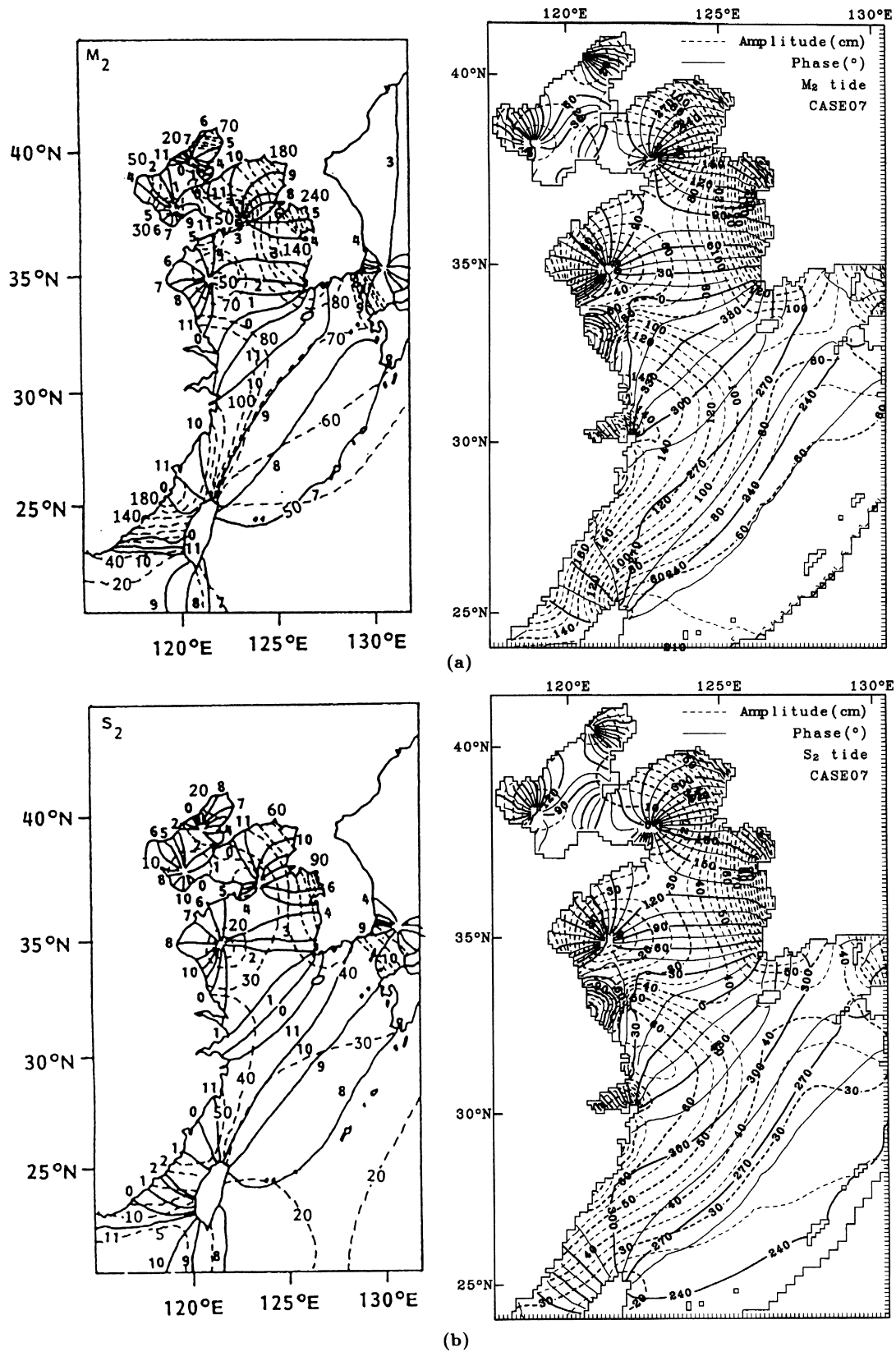
Fig. 2. The observed (left) and calculated (right) co-tidal (solid line) and co-range (broken line) charts of the M_2, S_2, K_1 and O_1 tides. The observed ones are after Yanagi and Inoue (1994), which are based on Nishida (1980).
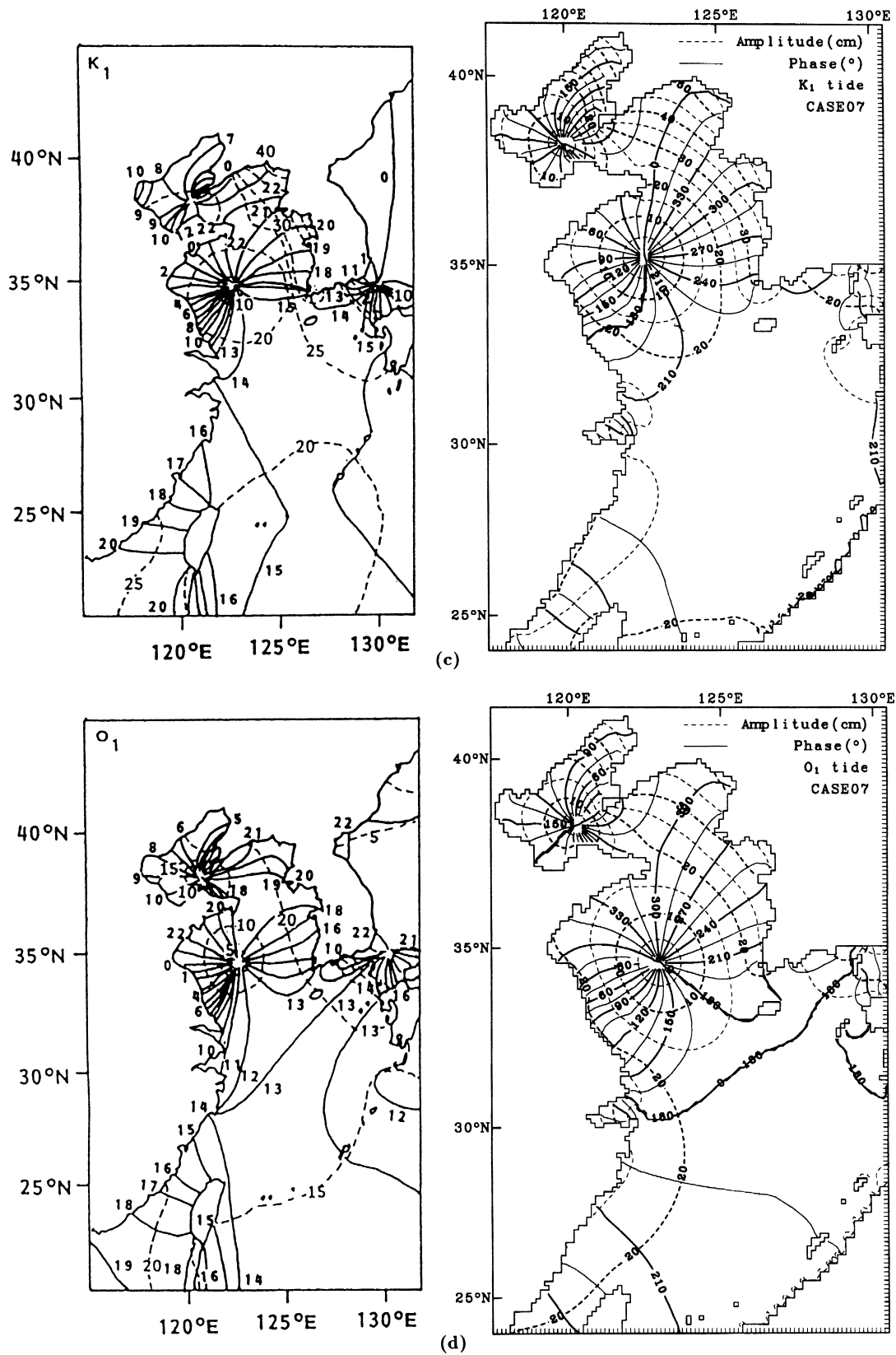
Fig. 2. (continued).
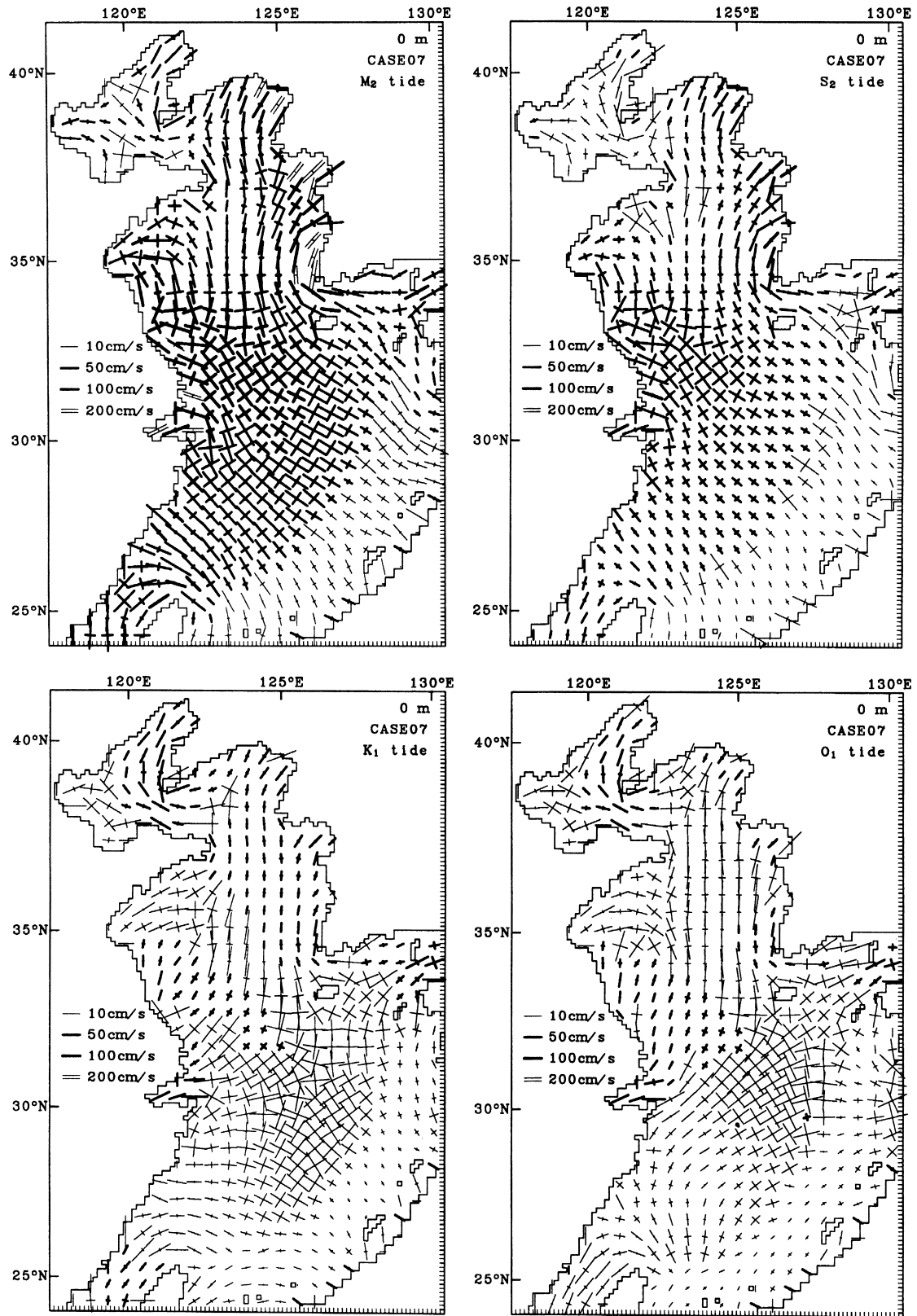
Fig. 3. The horizontal distribution of the M_2, S_2, K_1 and O_1 tidal current ellipses on the sea surface.

two-dimensional models (Choi, 1980; Zhao *et al.*,1994). As the results of a three-dimensional tidal model, we want to pay more attentions to the vertical variation of tidal current.

3.4 The vertical profiles of tidal current at some stations

Among 15 stations in Larsen *et al.* (1985) and Choi (1984, 1985, 1989), four stations are chosen to represent the shallow water, the continental shelf, the shelf edge and the Yellow Sea. The observed M_2 and K_1 tidal currents data and the vertical profile of calculated M_2 and K_1 tidal currents by four vertical eddy viscosity models are presented in Figs. 4 and 5, respectively.

3.4.1 M_2 tidal current

a. Shallow water

Stn. M2 represents the typical shallow water tidal current, with a depth of only 15 m and a very strong tidal current (60–100 cm/s). The calculated current there is very sensitive to the vertical eddy viscosity. The constant vertical eddy viscosity model (case 4) produces a large vertical current shear, while the other ones cause the current to vary smoothly from the sea bottom to the sea surface, as shown in the upper panel of Fig. 4. Such a difference is explained by the fact that the vertical eddy viscosity (50 cm^2/s) used in the constant model is so small that the bottom friction stress produces a large vertical current shear. In the HU (a) (case 7), HU (b) (case 8) and mixing length models (case 6), the calculated vertical eddy viscosities are large. So the bottom friction stress only produces a small current shear in the vertical.

b. Continental shelf

Stn. MS represents the tidal current on the continental shelf, whose depth is about 50 m and where the tidal current is relatively large (30–50 cm/s). Compared to Stn. M2, the calculated tidal current is not so sensitive to the vertical eddy viscosity. However, the constant vertical eddy viscosity model (case 4) gives an unnatural current profile below the mid-depth, as shown in the second panel of Fig. 4, which may be attributed to the small vertical eddy viscosity too. It should be noted that such an unnatural profile can also be found at Stn. M5, Stn. M7 and Stn. CM7. At these stations, the bottom friction stress is not so large as that at Stn. M2 due to the decrease of tidal current. And the increased depth means that the bottom friction stress only influences a small part of the water column, while at Stn. M2 it influences the whole water column. Consequently, the large vertical current shear only appears near the sea bottom. Beyond the range influenced by the bottom friction stress, there is no factor to produce the vertical shear. So the current tends to keep the same magnitude in the vertical direction. On the other hand, the other three models result in a large vertical eddy viscosity, which distributes the influence of the bottom friction stress to a large range of the water column and the current varies smoothly from the sea bottom to the surface.

c. Shelf edge

At the shelf edge (Stn. SB), the calculated current is not sensitive to the vertical eddy viscosity due to its weak tidal current, which produces a small bottom friction stress and a small vertical eddy viscosity in the HU (a) (case 7), HU (b) (case 8) and mixing length (case 6) models. However, the calculated current is smaller than the observed one, no matter what the *u* and *v* components are. Two possibilities may be considered. The first one is that the numerical model does not represent the topography there well. The second one is that the baroclinic tidal current accompanied by the internal tide is probably included in the observed data, but is not included in the numerical model. We prefer the second explanation because of the topography there and the period of observation (June, 1980).

d. Yellow Sea

Stn. F is located on the Yellow Sea, close to the western Korean coast. As shown in Fig. 3, the M_2 tidal current there has a strong north-south component, which can be found in Fig. 4 too, in which the *v* component is clearly larger than the *u* component. The vertical profile of the *v* component at this station is very similar to those on the continental shelf, and the constant vertical eddy viscosity model (case 4) produces the unnatural distribution, too. However, the *u* component at Stn. F shows a different profile. Its amplitude becomes large near the sea bottom. Such a profile is also shown in the observed data there and can be found in the calculated results at Stn. B, Stn. D and Stn. I too. A detailed discussion will be given below.

3.4.2 K_1 tidal current

The vertical distributions of K_1 tidal currents at four stations are shown in Fig. 5. On the whole, the K_1 tidal current is not sensitive to the change of the vertical eddy viscosity. In fact, since the K_1 tidal current is very much weaker than the M_2 tidal current, the vertical eddy viscosities calculated by the four models do not have such a great difference as those in the M_2 tide calculations. Also, as the current is weak, the bottom friction stress is small too, which in turn means a small vertical current shear. Thus, the unnatural vertical profile as seen in the M_2 tidal current at Stn. MS produced by the constant vertical eddy viscosity model does not appear here.

In the shallow water (Stn. M2), the K_1 tidal current has a relatively large variation with the change of the vertical eddy viscosity, as shown in Fig. 5. The HU (a) model (case 7) gives better results than the others. On the continental shelf (Stn. MS), the model overestimates the observed current somewhat. At the shelf edge (Stn. SB), the model reproduces the observed current well. In the Yellow Sea (Stn. F), the K_1 tidal currents have similar characteristics as the M_2 tidal current, that is, the *v* component is larger than the *u* component by one or two times and the *u* component becomes large near the sea bottom. We will discuss this issue in some detail later.
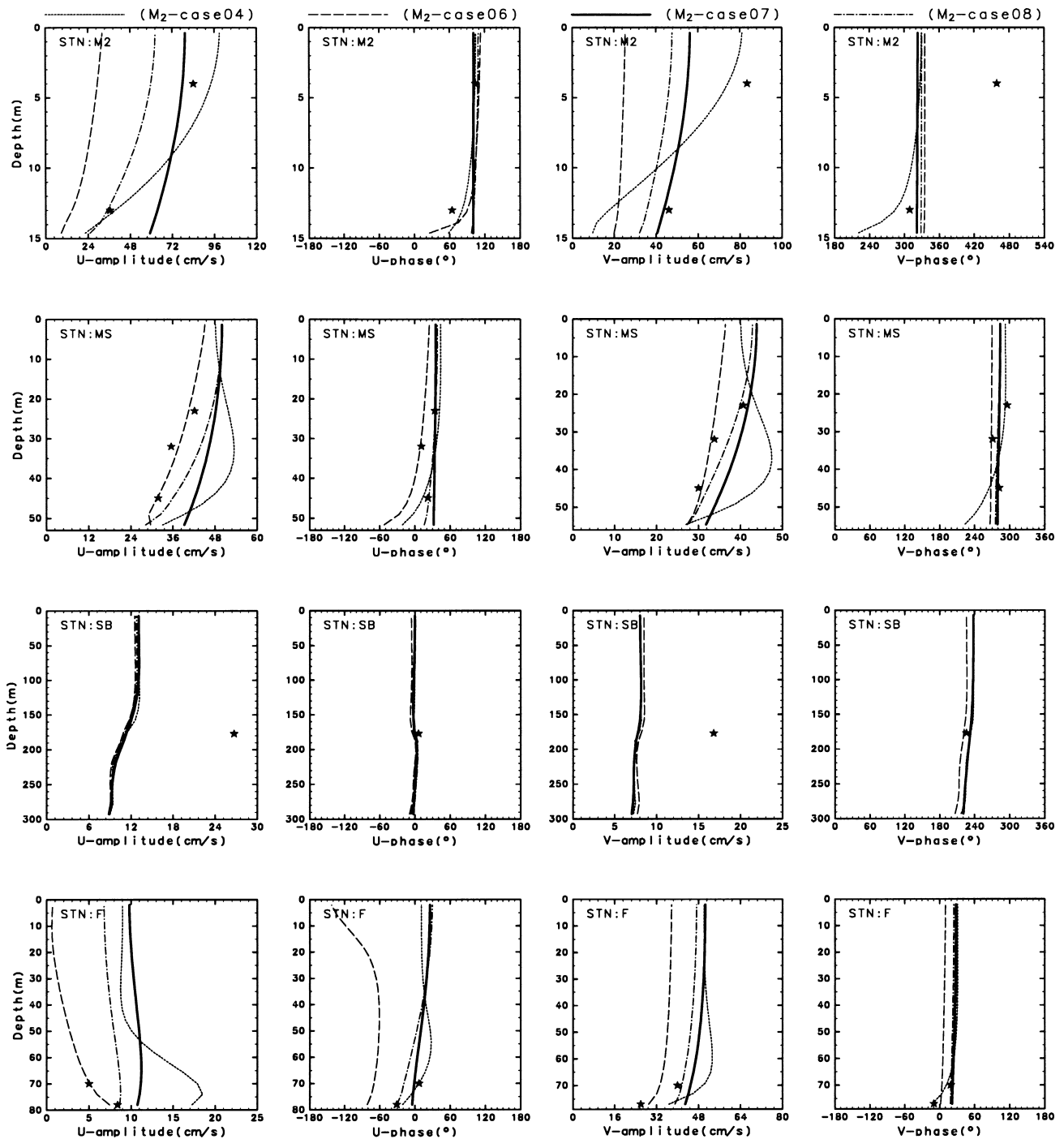
Fig. 4. The vertical profiles of the amplitudes and phases of *u* and *v* components of the M₂ tidal currents at 4 stations Stn. M2, Stn. MS, Stn. SB and Stn. F whose positions are shown in Fig. 1. The different types of line represent the results of different cases as shown above the upper panel. The observed tidal current data are shown by the black stars.

3.5 The vertical distribution of tidal current along a section

Although we know something about the vertical distribution of tidal current at some points, we still have no idea about the vertical distribution of tidal current over the whole domain. Therefore, we chose a vertical section in the domain

as shown in Fig. 6 to see how the tidal current varies along this section.

The amplitudes of *u* and *v* components of M₂ and K₁ tidal current calculated by the HU (a) model (case 7) is shown in Fig. 7. The regions where the vertical shear of
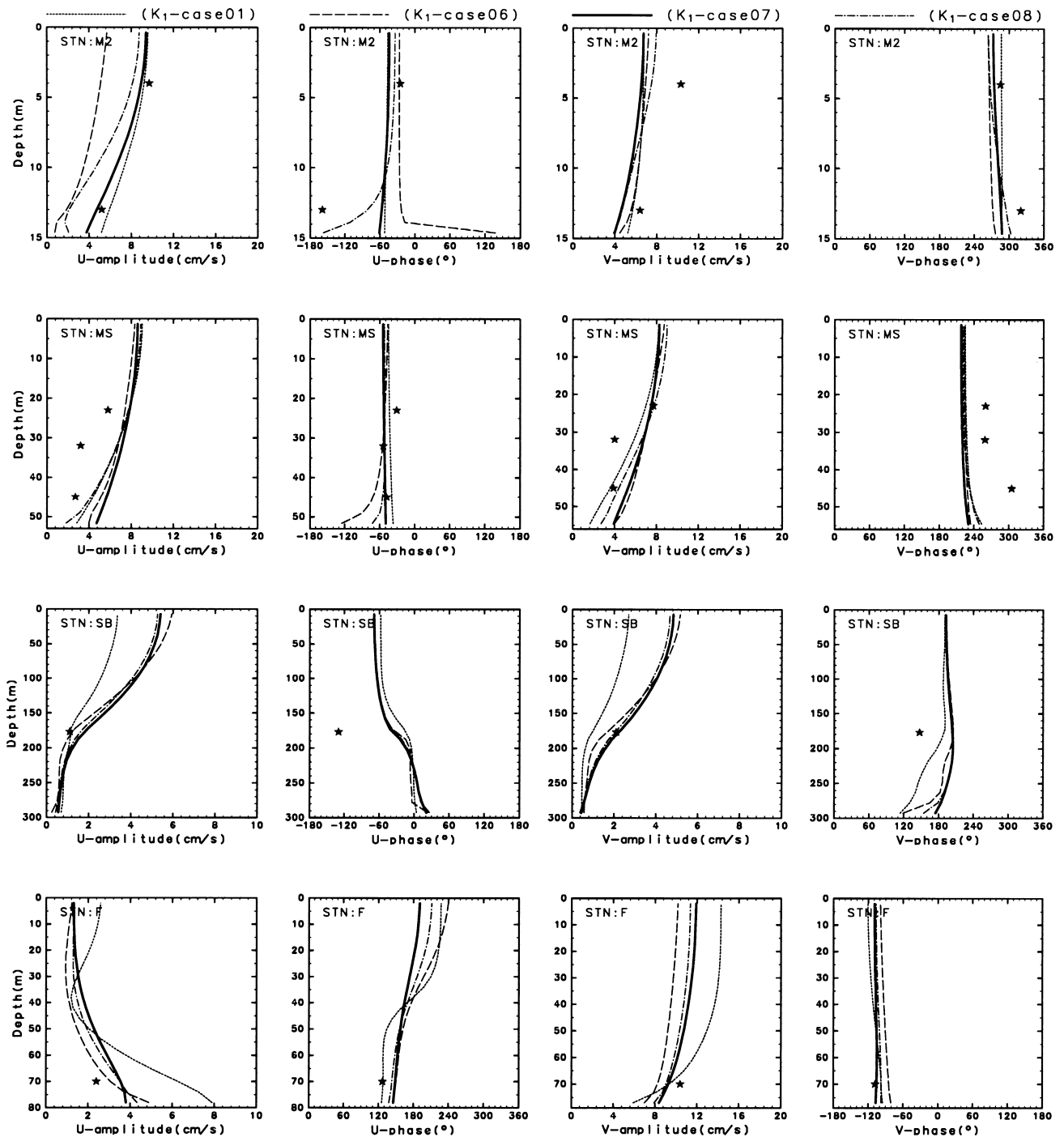
Fig. 5. The vertical profiles of the amplitudes and phases of *u* and *v* components of the K₁ tidal currents at the same 4 stations as Fig. 4.

current is large is section C–D for M₂ tidal current, section B–C for K₁ tidal current. Obviously, the current varies greatly in the vertical when the current itself is strong. So from the horizontal distribution of tidal current ellipses (Fig. 3), we can deduce the area where the vertical shear of tidal current is large.

4. Discussion

4.1 Reproduction of the amphidromic point in Liaodong Bay

There are only two different points in the calculations for the M₂ and S₂ tides. One is their periods and another is
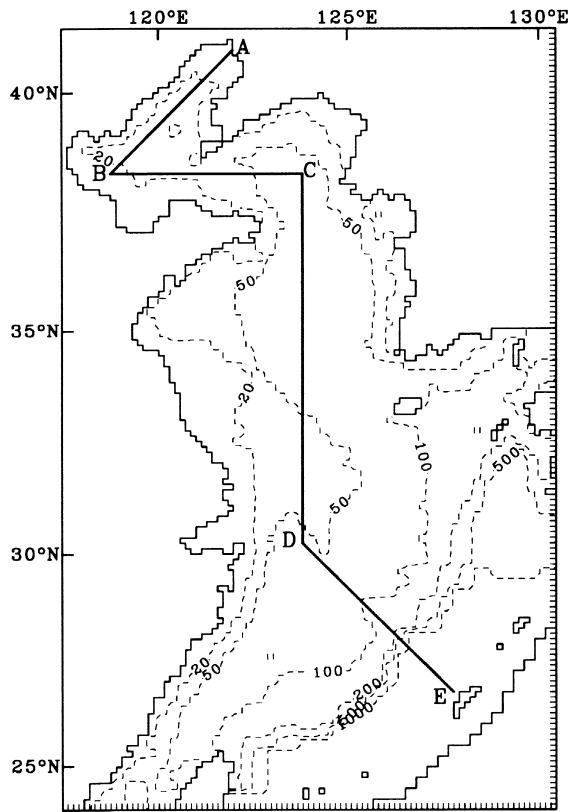
Fig. 6. The position of a chosen section along which the amplitude and phase of the M_2 and K_1 tidal currents are shown in Fig. 7.

the harmonic constants along the open boundary. The question is, why cannot the amphidromic point of M_2 tide in Liaodong Bay be reproduced in the large bed drag coefficient cases, while the amphidromic point of S_2 tide can be reproduced under the same bed drag coefficient? To answer this question, we performed the following two experiments, in which the bed drag coefficient is kept as 0.0025. The first one was to use the S_2 tidal period in the M_2 tide calculation. This calculation is the same as the S_2 tide simulation using the harmonic constants of M_2 tide along the open boundary. The result is that the amphidromic point in Liaodong Bay cannot be reproduced. The second experiment consisted of using the harmonic constants of S_2 tide along the open boundary in M_2 tide calculation. In this experiment, the amphidromic point in Liaodong Bay is reproduced.

So it is the harmonic constants along open boundary that influence the appearance of the amphidromic point in Liaodong Bay. We consider the physical explanation to be that the large amplitude of M_2 tide produces a strong tidal current, which in turn induces a larger bottom friction stress than the S_2 tide, if the same bed drag coefficient is used. This larger bottom friction stress moves the amphidromic point in Liaodong Bay from the central axis of the bay too far, that is, into the land. When the bed drag coefficient decreases or the tidal current becomes weak, the bottom friction stress decreases and the amphidromic point appears in Liaodong Bay.

In order to gain more support for this explanation, we carried out two further experiments using the M_2 tide period.

(a)
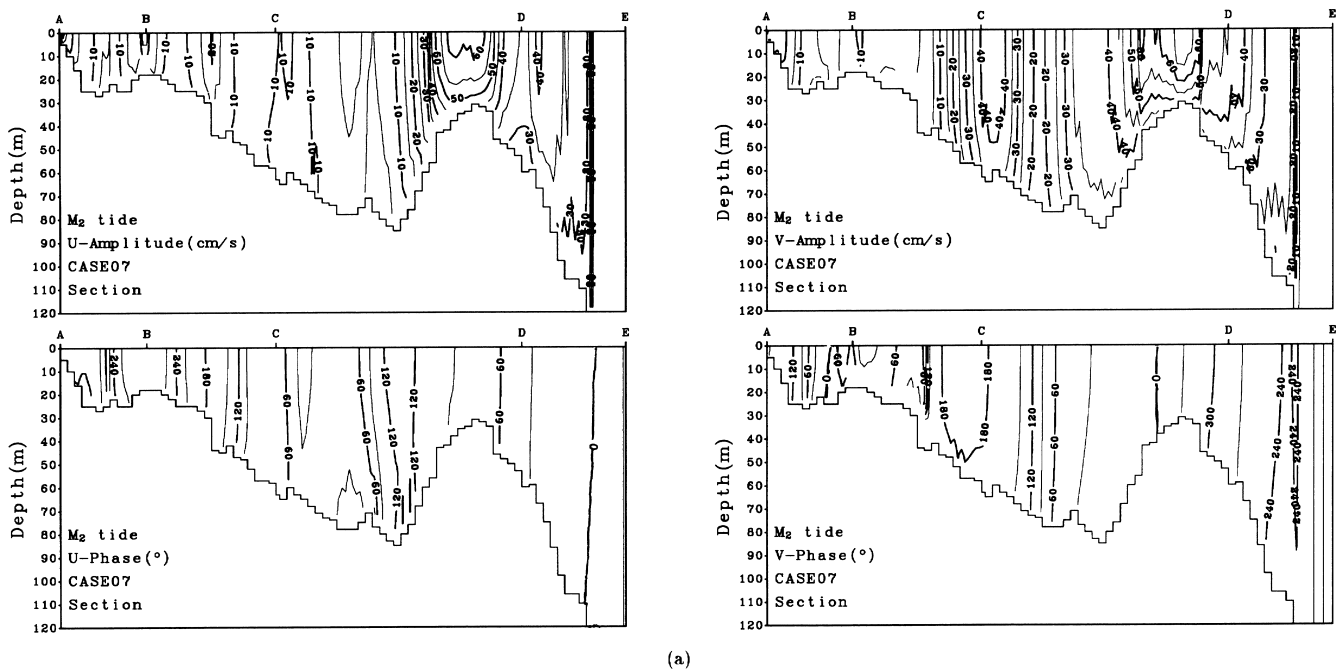
Fig. 7. The distributions of the amplitudes and phases of u and v components of M_2 tidal current (a) and those of K_1 tidal current (b).

The first one uses the S_2 tide phase data and the M_2 tide amplitude data along the open boundary. The second one uses the S_2 tide amplitude data and M_2 tide phase data along the open boundary. The bed drag coefficient is still kept as 0.0025. The calculated results show that the amphidromic point in Liaodong Bay cannot appear in the first experiment but can appear in the second experiment, which means that the phase data of M_2 or S_2 tide along the open boundary have little influence on the reproduction of the amphidromic point in Liaodong Bay, but the amplitude data along the open boundary, which in turn the tidal current and the bottom friction stress, influence the reproduction of that point mainly.

It was also stated that the poor grid resolution and the unnatural orientation of the grid system with respect to the coast's shape should be responsible for the failure in reproducing the amphidromic point in Liaodong Bay (Larsen *et al.*, 1985). However, the improvement of the model's resolution from 25 km to 12.5 km and the modification of the coastline using the fine grids did not introduce any clear improvement of the results over the calculated result using the coarse grids. Therefore the main factor influencing the reproduction of the amphidromic point of M_2 tide in Liaodong Bay should be the bottom friction stress.

4.2 The unique vertical profile of the tidal current at Stn. F

Usually, the tidal current becomes weak near the sea bottom due to the effect of bottom friction. The profiles of u component of tidal current at the stations in the Yellow Sea such as Stn. F are therefore unique. The question naturally arises of whether such profiles really exist in the nature and why the model can produce such profiles. In the present state of our knowledge, it is difficult to answer the first question because the observed data are scarce in the vertical. However, we may try to answer the second question by analyzing the calculated results in detail.

Using a linear model, the momentum equation about the u component, neglecting the horizontal viscosity, may be expressed as:

$$\frac{\partial u}{\partial t} = fv - g\frac{\partial \eta}{\partial x} + \frac{\partial}{\partial z}\left(A_v \frac{\partial u}{\partial z}\right). \tag{11}$$

The tidal current is controlled by the Coriolis force, pressure gradient and the vertical shear stress. In other words, it may be explained that the tidal current is driven by the sum of the three terms on the right, which are referred to as the driving force for convenience.

Figure 8 shows the u component of tidal current and the driving force over one tidal period at Stn. M2 and Stn. F. These results are obtained in case 4 for M_2 tide without the advective and horizontal viscosity terms. The periodic variations of the current and the driving force and the 90 degree phase difference between them may be found clearly at both stations. The difference between the two stations is the vertical distribution of the current and the driving force. From Eq. (11), we know that a strong tidal current must be
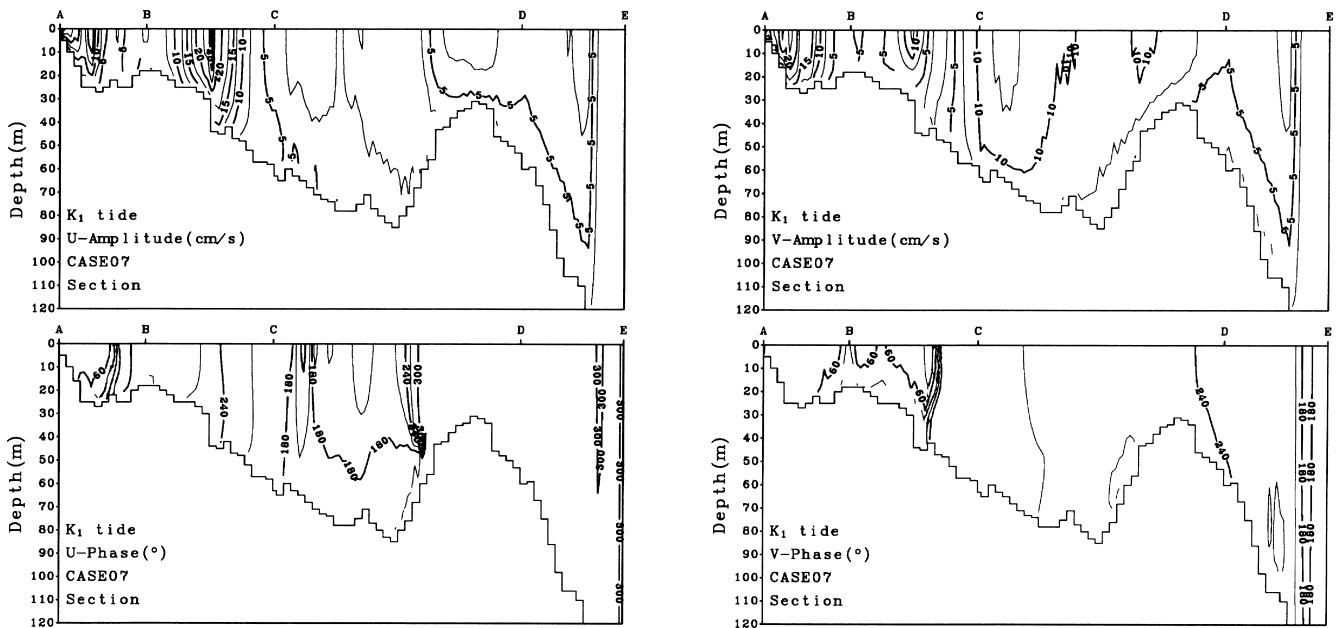
(b)

Fig. 7. (continued).
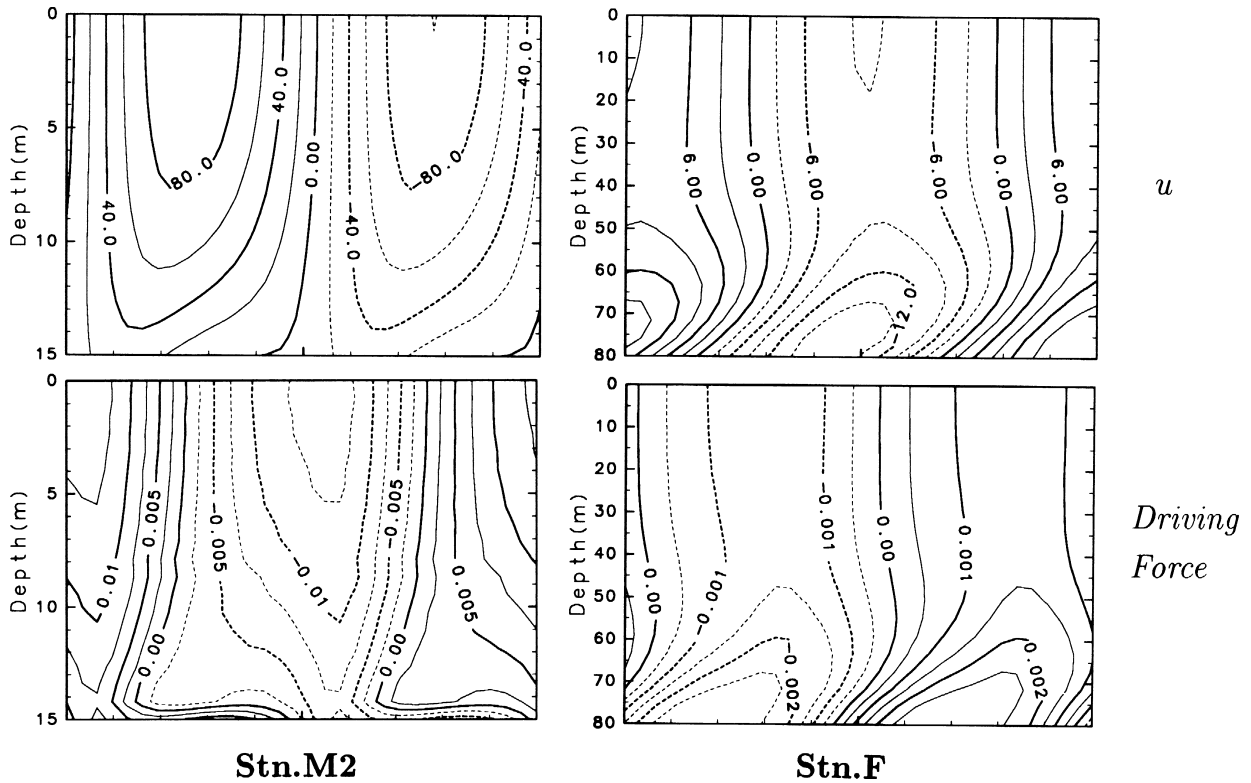
Fig. 8. The time variations in the M$_2$ tidal cycle of the u component and the driving force in the x direction at Stn. M2 and Stn. F in the case 4.

driven by a large driving force, while a small driving force may only produce a weak tidal current. The vertical distributions of the driving forces and their corresponding current in Fig. 8 explain this rule very well.

To find the reasons responsible for the large bottom driving force at Stn. F, the time variation of the Coriolis force, the pressure gradient, the difference between them and the vertical shear stress at Stn. M2 and Stn. F are plotted in Fig. 9. The variations of Coriolis force and pressure gradient themselves have no special characteristic. But their differences, especially the vertical distribution of their difference at the two stations, are very clear. Because the u component at Stn. F is small, the vertical shear stress there caused by the bottom friction stress is small too, and less than the difference of Coriolis force and pressure gradient by one order. On the other hand, the v component at Stn. F is large, which induces a large Coriolis force in the u direction. It may be said that the force balance at Stn. F is mainly the balance between the pressure gradient and the Coriolis force. Therefore, the phase difference between the Coriolis force and the pressure gradient and the decrease of the Coriolis force near the sea bottom are the reasons responsible to the large driving force at the sea bottom of Stn. F, which in turn produces a strong tidal current there. It should be noted that this unique profile is reproduced in

cases 9–12 too.

The thickness of the bottom Ekman layer (BEL) relates to this unique profile too. As the vertical eddy viscosity near the bottom is as small as that in K$_1$ tide simulations and cases 4 and 6 of M$_2$ tide simulations, the BEL is thin. Then the u component of tidal current becomes large near the bottom. But in the cases 7 and 8 of M$_2$ tide simulations, the vertical eddy viscosity near the bottom is large and makes the thickness of BEL large too. So the unique profile cannot be reproduced.

4.3 Summary of the four vertical eddy viscosity models

Concluding the results of the four vertical eddy viscosity models, we know that the constant vertical eddy viscosity model may be used in the shallow water, where the tidal current is very strong and the current shear is large. As the water depth increases and the tidal current become weak, the constant vertical eddy viscosity model produces an unnatural current profile near the sea bottom. Of course, by changing the value of the constant, this unnatural current profile may disappear. But it should be difficult for the constant vertical eddy viscosity model to reproduce the correct vertical profile of tidal current on the whole continental shelf well.

As for the mixing length model, it usually underestimates tidal current amplitude because it produces a large
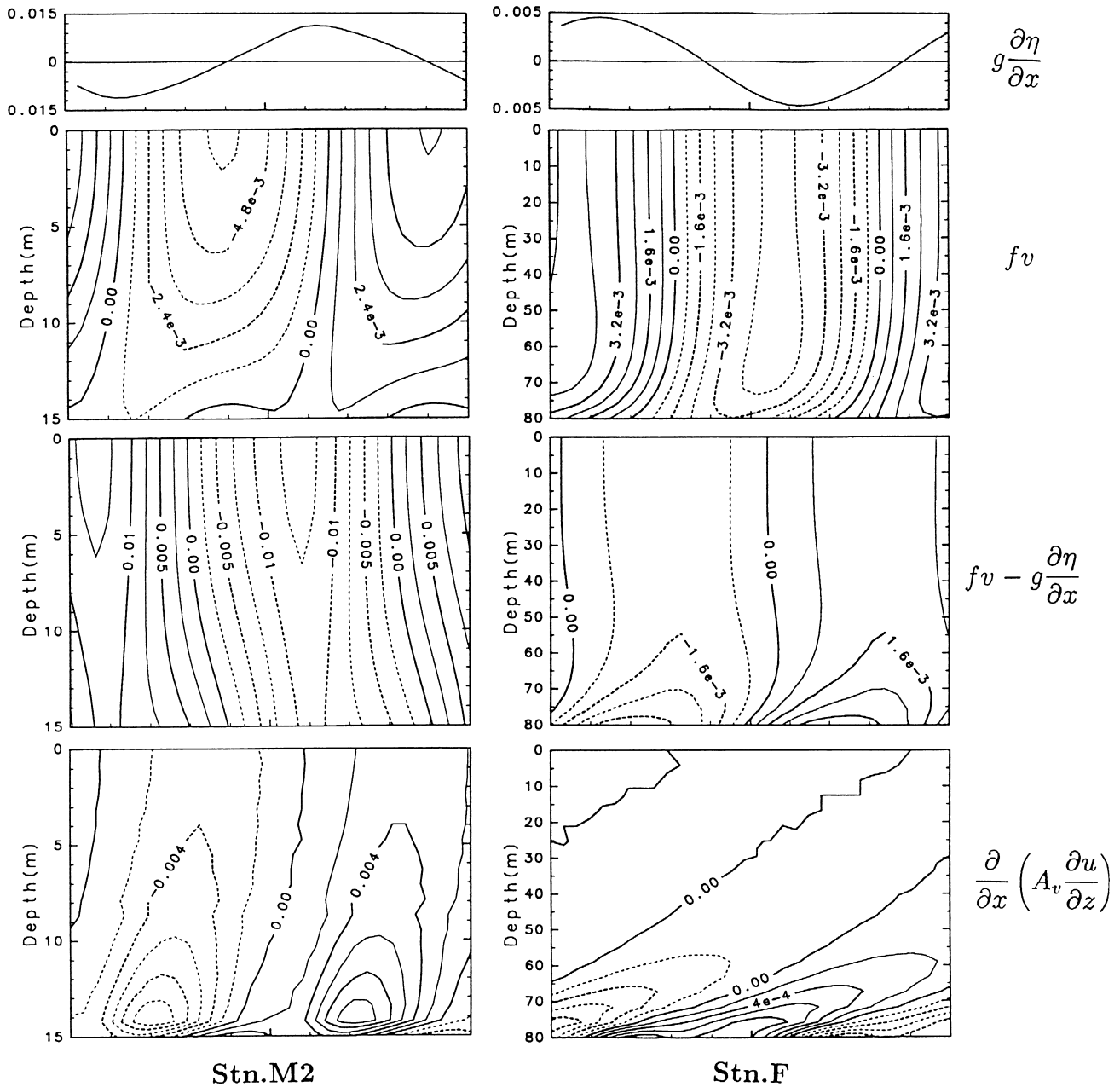
Fig. 9. The time variations in the M$_2$ tidal cycle of the pressure gradient, the Coriolis force, their difference and the vertical shear stress in x direction at Stn. M2 and Stn. F in the case 4.

interior friction on the continental shelf. In fact, deciding the mixing length is the key point of this model. Since the mixing length is basically proportional to the water depth, a small current shear may produce a very large vertical eddy viscosity in the deep water. Therefore, before we know more about the mixing length, this model is not recommended for use to simulate the tide and tidal current on the continental shelf. At least, it is not suitable for the ECS and the Yellow Sea.

As for the HU models, their performances are relatively good. Compared to the HU (a) model, model HU (b) produces a large vertical current shear near the sea bottom, but cannot produce the amphidromic point of M$_2$ tide in Liaodong Bay. Therefore, as a conclusion, the HU (a) model is thought to be the best vertical eddy viscosity model for simulating the tide and tidal current in the ECS, the Yellow Sea and the Bohai Sea.

5. Conclusion

Using a high resolution three-dimensional numerical model, the tides and tidal currents of M_2, S_2, K_1 and O_1 constituents in the ECS and the Yellow Sea are reproduced well. With 12.5 km resolution in the horizontal and 20 layers in the vertical, the model presents the vertical distribution of tidal currents in the ECS and the Yellow Sea for the first time.

Four vertical eddy viscosity models are used in the numerical experiments. As the tidal current becomes strong, its vertical shear becomes large and its vertical profile becomes sensitive to the vertical eddy viscosity model. As a conclusion, the HU (a) model, which relates the vertical eddy viscosity to the water depth and depth mean velocity, gives the closest results to the observed data.

The reason for the reproduction of the amphidromic point of M_2 tide in Liaodong Bay has been discussed and is attributed to the bottom friction stress calculation. The model reproduces a unique vertical profile of tidal current in the Yellow Sea, which is shown in the observed data too. The reason for producing such a profile in the model has been investigated.

Due to the limitations of the observed data, especially the observed tidal current data, some of the model results cannot be verified in detail. On the other hand, it remains a problem to be solved in the future, to include the baroclinic tide and tidal current in the numerical model and to improve the precision of topography data.

References

An, H. S. (1977): A numerical experiment of the M_2 tide in the Yellow Sea. *J. Oceanogr. Soc. Japan*, **33**, 103–110.

Choi, B. H. (1980): A tidal model of the Yellow Sea and the eastern China Sea. KORDI Report 80-02, 72 pp.

Choi, B. H. (1984): A three-dimensional model of the East China Sea. p. 209–224. In *Ocean Hydrodynamics of the Japan and East China Seas*, ed. by T. Ichiye, Elsevier, Amsterdam.

Choi, B. H. (1985): Observed and computed tidal currents in the East China Sea. *J. Oceanogr. Soc. Korea*, **20**, 56–73.

Choi, B. H. (1989): A fine-grid three-dimensional M_2 tidal model of the East China Sea. p. 167–185. In *Modeling Marine Systems*, ed. by A. M. Davies.

Davies, A. M., S. C. M. Kwong and R. A. Flather (1997): Formulation of a variable-function three-dimensional model, with application to the M_2 and M_4 tide on the North-West European Continental Shelf. *Cont. Shelf Res.*, **17**, 165–204.

Ding, W. (1984): A study on the characteristics of the tide and tidal current in the East China Sea. *Studia Marinea Sinica*, **21**, 135–148 (in Chinese).

Fang, G. (1986): Tide and tidal current charts for the marginal seas adjacent to China. *C. J. of Oceanology and Limnology*, **4**, 1–16.

Fang, G. and T. Ichiye (1983): On the vertical structure of tidal currents in a homogeneous sea. *Geophys. J. R. Astr. Soc.*, **73**, 65–82.

Guo X. and T. Yanagi (1994): Three dimensional structure of tidal currents in Tokyo Bay, Japan. *La mer*, **32**, 173–185.

Larsen, L. H., G. A. Cannon and B. H. Choi (1985): East China Sea tide currents. *Cont. Shelf Res.*, **4**, 77–103.

Nishida, H. (1980): Improved tidal charts for the western part of the north Pacific Ocean. *Report of Hydrographic Researches*, **15**, 55–70.

Ogura, S. (1933): The tides in the sea adjacent to Japan. *Bulletin of the Hydrographic Department, Imperial Japanese Navy*, **7**, 1–189.

Shen, Y. (1980): Numerical computation of tides in the East China Sea. *Journal of Shandong College of Oceanology*, **10**, 26–35 (in Chinese with English abstract).

Xing, J. and A. M. Davies (1996): Application of turbulence energy models to the computation of tidal currents and mixing intensities in shelf edge regions. *J. Phys. Oceanogr.*, **26**, 417–447.

Yanagi, T. and K. Inoue (1994): Tide and tidal current in the Yellow/East China Seas. *La mer*, **32**, 153–165.

Yanagi, T., A. Morimoto and K. Ichikawa (1997): Co-tidal and co-range charts for the East China Sea and the Yellow Sea derived from satellite altimetric data. *J. Oceanogr.*, **53**, 303–310.

Ye, A. and L. Mei (1995): Numerical modeling of tidal waves in the Bohai Sea, the Huanghai Sea and the East China Sea. *Oceanologia et Limnologia Sinica*, **26**, 63–70 (in Chinese with English abstract).

Zhao, B., G. Fang and D. Chao (1994): Numerical simulations of the tide and tidal current in the Bohai Sea, the Yellow Sea and the East China Sea. *Acta Oceanologica Sinica*, **16**, 1–10 (in Chinese).